Available online at www.sciencedirect.com
ScienceDirect
International Journal of Mass Spectrometry 269 (2008) 196–209
International Journal of Mass Spectrometry
www.elsevier.com/locate/ijms

Vibrational signatures of sodiated oligopeptides (GG–Na^+, GGG–Na^+, AA–Na^+ and AAA–Na^+) in the gas phase

O.-P. Balaj [a], C. Kapota [a], J. Lemaire [b], G. Ohanessian [a,*]

[a] *Laboratoire des Mécanismes Réactionnels, Département de Chimie, Ecole Polytechnique, CNRS, 91128 Palaiseau Cedex, France*
[b] *Laboratoire de Chimie Physique, Université Paris-Sud 11, CNRS, 91405 Orsay Cedex, France*

Received 6 July 2007; received in revised form 12 October 2007; accepted 15 October 2007
Available online 23 October 2007

Abstract

The structures of the sodium complexes of oligoglycines (GG–Na^+, GGG–Na^+) and oligoalanines (AA–Na^+, AAA–Na^+) have been studied by infrared spectroscopy in the gas phase. Two different experimental set-ups have been used to generate, trap and analyze the ions. In the first, the complexes were generated by MALDI and analyzed in the cell of a home built FT-ICR mass spectrometer. In the second an external electrospray source was coupled to a Paul type ion trap. Following their trapping, the ions are irradiated in both cases with intense, tunable infrared light in the 1000–2000 cm^{-1} range, leading to sodium ion detachment and ion fragmentation via the absorption of multiple photons. The resulting experimental spectra are compared to theoretical linear absorption spectra to assign structures. In agreement with calculations, peptide attachment to Na^+ is found to have a strong structuring effect: the lowest energy structures involve binding of all carbonyl oxygens to the cation. Detailed comparison of experimental and computed spectra shows that the IRMPD spectroscopy of such gaseous ions allows the differentiation between structures which do not have the same number of carbonyl oxygens bound to Na^+, and structures in which the peptide is either wrapped around the ion or capped by it.

Keywords: IRMPD; Sodium; Oligoglycine; Oligoalanine; Mass spectrometry

1. Introduction

Mass spectrometry has been shown over the years to be able to detect and analyze molecules of virtually all types, with high selectivity and sensitivity. While the information on ion mass is extremely reliable, only limited information on the structure of gaseous ions can be obtained. Many approaches have been developed in order to infer structural features, including low- and high-energy collision-activated dissociation, specific ion–molecule reactions and ion mobility among others. Yet none is of general use and and they provide limited direct information on the three-dimensional structures, including functional group identification to distinguish between isomers, hydrogen bonding patterns, and local interactions of charged sites.

Another approach started to be recently explored with the coupling of infrared spectroscopy to mass spectrometry. The manipulation of ions in the gas phase is easy, ions can be selected in mass before being spectroscopically characterized, however the ion densities are small. As a result classical absorption spectroscopy through the measurement of the photon attenuation cannot be achieved. A kind of action spectroscopy has to be used, probing the photon absorption by monitoring its consequence on the mass spectrum. The absorption of photons increases the internal energy of the ions and it may lead to ion fragmentation if the number of absorbed photons is sufficient. Detecting such fragment ions, even when present in very small quantities, is made possible by the high sensitivity of mass spectrometry. Using ion trap devices such as RF traps or Fourier transform-ion cyclotron resonance (FT-ICR) traps it has been shown that the multiple photons absorption spectra of gaseous ions in the IR can be obtained and yields structural information in a way very similar to the more traditional one photon IR absorption spectroscopy.

As the energy required for dissociation is often much higher than the energy of a single photon, the ions must absorb up to

* Corresponding author at: Laboratoire des Mécanismes Réactionnels - UMR CNRS 7651, Département de Chimie - Ecole Polytechnique, 91128 Palaiseau Cedex, France. Tel.: +33 1 69 33 35 03; fax: +33 1 69 33 30 41.
E-mail address: gilles.ohanessian@polytechnique.fr (G. Ohanessian).

1387-3806/$ – see front matter © 2007 Elsevier B.V. All rights reserved.
doi:10.1016/j.ijms.2007.10.004

several tens of IR photons in order to fragment. This is made possible when using intense laser sources allowing for infrared multiple-photon dissociation (IRMPD). Although IRMPD was evidenced as early as 1978 [1], subsequent studies were severely limited by the wavelength range and tunability of the available laser sources. With the advent of infrared free electron lasers (IR FEL) in 1981, sources offering both wide tunability and high peak power became available. The free electron laser facilities CLIO [2] and FELIX [3] offer an output in the 500–2500 cm^{-1} range, making them very well suited for IRMPD experiments.

The first IRMPD spectra of gaseous ions using a FEL were obtained for polyaromatic ions at FELIX [4]. In the following years, a rapidly growing number of studies on organic, organometallic and biological molecular ions showed that the IRMPD technique using a FEL is a powerful tool yielding structural information, allowing to distinguish between isomers and sometimes also conformers for a wide range of ion types [5–28].

Due to their biological relevance as models of structural or catalytic sites in proteins, the structure of cationized amino acids and peptides have been studied before using other mass spectrometric techniques [29–44], but there was limited and sometimes contradictory evidence on the gas phase structures (or the cation structuring effect). Recently several IRMPD studies focused on such species, in order to get a direct structural identification from their vibrational fingerprints. The working strategy consists in comparing the recorded experimental "action" spectrum and the absorption spectrum predicted by *ab initio* or DFT calculations.

In the case of sodiated amino acids, the remarkable agreement between the two, allowed for a clear identification of the salt-bridge (SB) isomer in the case P–Na^+ [6]. In contrast, for G–Na^+ the charge solvation (CS) structure is favored [6]. Analogous conclusions in favor of charge solvation structures were reached for F–K^+ and Y–K^+ in the fingerprint range [9], and for W cationized with all five alkali cations [7]. For W–Na^+, it was further shown that H/D exchange via ion–molecule reaction with a neutral molecule such as CH_3OH or NH_3 may induce isomerization between CS and SB isomers [8]. A CS-type structure has also been determined for V–Li^+, however in this latter case experiments were carried out in the N–H/O–H stretch range [45]. The stepwise hydration of the V–Li^+ was shown to occur preferentially at the lithium ion for addition of the first three water molecules [45]. Even more recently, a SB structure was inferred for R–Na^+ in the same frequency range [46].

Experiments were also carried out on the potassiated peptides bradykinin fragments 1–5 (RPPGF) and [L]-enkephalin (YGGFL) [9]. Although spectral congestion was larger than for amino acid complexes, charge solvation vs. salt bridge structures appeared to remain distinguishable. While for the potassium tagged bradykinin fragments 1–5 the IRMPD spectrum suggests a SB structure, there is evidence that the potassium tagged [L]-enkephalin seems to favor a CS although the presence of some SB ions could not be excluded. Even for the large (104 amino acids) K^+-tagged multi-charged cytochrome c protein, the IRMPD spectrum displays clear bands in the amide I and II regions [11]. The spectra clearly showed a structural change as a function of the protein charge state. Deconvolution of the amide I band, as is usually done for absorption spectra recorded in solution, was found to be compatible with the existence of a helical portion [11].

In the present study we describe the IRMPD results obtained for small sodiated oligopeptides (GG–Na^+, GGG–Na^+, AA–Na^+ and AAA–Na^+) using two different experimental setups. We also explore the capabilities of IRMPD to differentiate between three-dimensional structures of these ions.

2. Experimental and computational methods

2.1. Infrared free electron laser (IR FEL) and mass spectrometer (MS) operation parameters

The ions have been generated and analyzed using two experimental setups, a transportable FT-ICR mass spectrometer called MICRA [48,49] and a modified Bruker Esquire 3000+ ion trap mass spectrometer [25] coupled to the FEL.

The IR FEL CLIO is based on a linear electron accelerator delivering electron kinetic energies in the 10–50 MeV range, and an undulator placed in an optical cavity. Electrons generate IR light in the cavity, and continuous tunability over a large spectral range ($\Delta\lambda/\lambda = 2.5$) is obtained by scanning the undulator gap. By tuning the length of the optical cavity, the FEL bandwidth can be adjusted. The laser wavelength profile was monitored, at each reading while recording the spectra, with a monochromator associated with a pyroelectric array detector (Spiricon^{TM}). The accessible wavelength range goes from 3 to 120 μm and has a high peak power (20 MW per micropulse, 3 kW per macropulse), well suited for IR multiple photon dissociation studies. In the present experiments, the long-wavelength cutoff was ca. 19 μm due to the absorption of the ZnSe entrance window. The light is delivered in 8 μs long macropulses fired at a repetition rate of 25 Hz. Each macropulse contains 500 ps long micropulses. The mean IR power was about 500 mW corresponding to micropulse and macropulse energies of 40 μJ and 20 mJ, respectively. For the experiments described herein, we have used an electron energy of 45 MeV which allows access to wavelengths in the 1000–1900 cm^{-1} range.

The first experimental set-up, MICRA, is a FT-ICR mass spectrometer based on a modified cubic cell situated in a 1.24 T permanent magnet. With the magnet geometry used the ions must be generated either in the cell or near the cell. The MALDI sample was deposited on a stainless steel holder, which was mounted 6 mm away from the middle of one of the trapping plate. The ions formed by laser vaporization of the MALDI sample with a non-focalized Nd:YAG laser enter the ICR cell, are stored with a background gas pressure of ca. 10^{-9} mbar for about 1 s, mass selected and then exposed to the FEL light. The infrared laser beam is focused in the middle of the ICR cell with a 1 m focal length spherical mirror. Although the laser beam dimension in the middle of the cell is smaller than the ion cloud, when irradiating ions for more than 1 s photo-fragmentation ratios as high as 80% can be observed, indicating that most ions eventually interact with the IR beam. The irradiation time is controlled by a fast electromechanical shutter, synchronized with the FEL. In the present study, peptide–Na^+ ions were mass selected 600–800 ms after their formation, irradiated with the

IR beam for one to a few seconds, the resulting ions were then detected and the cell emptied by applying a quench pulse on the trapping plates. Such a sequence was repeated 25 times, and the mass spectrum was the Fourier transform of the accumulated ion signal. Due to difficulties in producing the ions for a long time by MALDI, the IRMPD spectrum is the result of multiple scans, using smaller scan steps ($10\,cm^{-1}$) in the region of the IRMPD bands.

The second experimental set-up is based on a modified Bruker Esquire 3000+ ion trap mass spectrometer. The modification consists in a 0.7 mm hole drilled in the ring electrode to allow the irradiation of the ions with the focalized CLIO beam. The ions are generated by an electrospray ion source, transferred from atmospheric pressure to the trap by two octopoles. Upon entering the trap the ions are stabilized by collisions with the He bath gas at a pressure of 10^{-3} mbar. After a rapid thermalization the ions are confined in a very small volume in the center of the trap. Following a 0.5 s relaxation time, they are mass selected and fragmented by one to five macropulses of IR light. As a direct consequence, there is a better overlap of the ion cloud with the IR FEL light than in the ICR cell, resulting in increased fragmentation efficiency. The 1000–1900 cm^{-1} wavenumber range was obtained using an electron energy of 45 MeV.

In the case of the FT-ICR experiments, the IRMPD spectra are plotted using the fragmentation yield R defined as: $R = -\log[I_{Parent}/(I_{Parent} + \Sigma I_{Fragment})]$. In the case of the ion trap experiments this was not possible as we were not able to observe the primary fragment and parent depletion spectra are presented. Depletion IRMPD spectra are intrinsically more noisy than fragmentation IRMPD spectra since ion signal fluctuations appear directly in the absolute, rather than relative intensities used. This is why the spectra derived from the ion trap experiments are of lower quality than those from FT-ICR experiments in the present case.

2.2. Sample preparation

The samples used for MICRA experiments were prepared as described in detail elsewhere [6]. For those experiments the ions were produced internally by MALDI using a pulsed Nd:YAG laser at tripled frequency of 355 nm. The best signals were obtained using a four-layer sample prepared using the sandwich technique [47]. The first and fourth layers were deposited from the solution of a matrix dissolved to 3.75×10^{-2} mol/L. We have mainly used as matrix the 4-hydroxy-α-cyano cinnamic acid (4-HCCA) in 1/3 water/acetone solvent. In the case of GGG–Na^+ the 2,5-dihydroxy benzoic acid (DHB) in water was preferred, due to the mass similarity of 4-HCCA–Na^+ and the sodiated peptide molecular ion. The NaCl was deposited in the second layer from a 10^{-2} mol/L aqueous solution while the peptides were deposited in the third layer in the same conditions as NaCl. Each new layer was allowed to dry before the next was added.

In the case of ion trap experiments, the ions were obtained by electrospray of diluted sample solutions. First, 10 mL peptide stock solutions were prepared using 1 mL 10% formic acid and 9 mL H_2O/MeOH 50:50 in order to dissolve the 10 mg of solid peptide. Ten to 50 μL of stock solution (10^{-3} M) were mixed 1:1 with NaCl solution (10^{-3} M) and diluted to 1.0 mL with H_2O/MeOH 50:50 with 2% formic acid. This protocol produced samples with concentrations of peptide in the μM range, leading to the formation of the sodiated peptide ion as the dominant species in the gas phase.

2.3. Computational details

The structures of all sodiated peptides considered herein have been studied previously [37,50–54]. In our previous work [52–55], preliminary Monte Carlo searches using the Amber94 force field were used to explore the potential energy surfaces, leading to a large number of structures. A subset of these structures was then subjected to geometry optimization at the Hartree Fock level with the 6-31G(d) basis set, and final energetics were obtained at the MP2(full)/6-311+G(2d,2p)//HF/6-31G(d)) level. Geometry optimization at the MP2/6-31G(d) level was used as well. In that work our focus was on the sodium–peptide interaction energies, while here calculations are used to assign IRMPD spectra. Hybrid DFT methods such as B3LYP have been shown to outperform HF and MP2, as well as local or gradient-corrected DFT, in predicting infrared intensities [56]. Thus we have used B3LYP calculations to re-optimize geometries and obtain vibrational spectra, at the B3LYP/6-31G(d) level. Although not of direct interest, refined energetics were calculated at the B3LYP/6-311+G(2d,2p)//B3LYP/6-31G(d) level. There are some differences found between the various levels used, for instance relative energies may differ by up to 5–7 kJ mol^{-1}. However the features that are relevant to the present study remain unchanged, i.e., that the lowest energy structures have all carbonyl groups interacting with Na^+, and the assignment of the experimental bands are the same. All calculations used the Gaussian03 package [57].

A scaling factor of 0.96 was applied to B3LYP/6-31G* frequencies as is commonly done in the 1000–2000 cm^{-1} region. The same scaling factor was derived from the comparison of experimental and B3LYP/6-31G* frequencies in the 800–1800 cm^{-1} range in the IRMPD spectra of Fe(I) complexes [48,49].

3. Results and discussion

3.1. Calculated structures

3.1.1. GG–Na^+

The sodium cation favors electrostatic interactions therefore binding to the polar carbonyl groups is most favorable. Binding to the terminal amine is also possible. Three conformers of low energy were identified in our calculations and their structures are presented in Fig. 1 following the nomenclature used in Ref. [52]. The conformer Gly_2–Na^+ **I** has a coordination of sodium with the two oxygens and with the terminal amine. Since the coordination of sodium is pyramidal, it is a stereogenic center. A number of structures thus exist as pairs of enantiomers. In structure **II** the sodium ion is coordinated only to the two oxygens

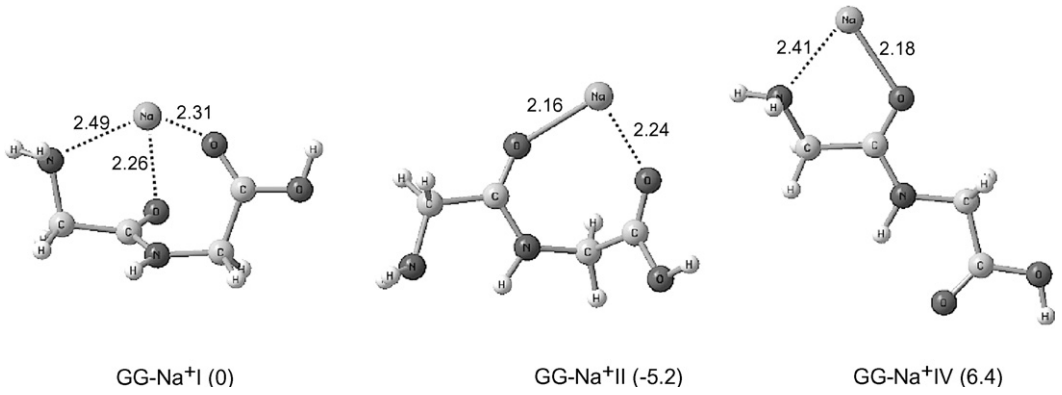

Fig. 1. Computed structures for the most stable structures of GG–Na^+ at the B3LYP/6-31G* level. The enthalpies (relative to that of structure **1**) are in kJ/mol, as calculated at the B3LYP/6-311+G(2d,2p)//B3LYP/6-31G* level. Bonds distances are given in Å.

(O^1O^2), while the N atom of the terminal amine interacts with the hydrogen of the peptide amide forming a five-membered C_5 motif ($N^2H \rightarrow N^1$). Finally, in conformer **IV**, the sodium is coordinated only to one residue by the terminal amine and the peptidic carbonyl (O^1N^1). The structure is analogous to structure CS1 of G–Na^+ [6] with the second residue bearing a hydrogen bond between the amide hydrogen and the carbonyl oxygen of the acid forming a C_5 cycle ($N^2H \rightarrow O^2$).

The energetics were calculated at the B3LYP/6-311+G(2d,2p)//B3LYP/6-31G* level. The two lowest energy conformers are **I** and **II**, with **II** slightly more stable while the reverse ordering was obtained at the MP2 level. At both levels, structure **IV** is higher in energy. In conclusion the most stable structure has both carbonyl oxygens bound to sodium, and the conformation at the N terminus leads to two conformations of similar energies.

3.1.2. AA–Na^+

The three most stable structures of AA–Na^+ are very similar to those of GG–Na^+. In most cases these conformers exist as pairs, because the sodium is a stereogenic center. Structures and relative energies of the most stable of each pair of stereoisomers are presented in Fig. 2. All methods indicate that as for GG–Na^+, **I** and **II** have similar energies, however **I** is found to be more stable in the present case. Again **IV** has the highest energy.

Although the structures of AA–Na^+ and GG–Na^+ are very similar, the metal–ligand distances are slightly shorter (0.01 Å) in the case of AA–Na^+. This effect could be due to donor character of the methyl groups, slightly increasing the nucleophilic character of the oxygens and to the higher polarizability of the methyls compared to hydrogen atoms.

3.1.3. GGG–Na^+

The structure of the most stable conformers of GGG–Na^+ have been published recently [54], yet there is no comprehensive picture available to date. Therefore, we have explored extensively the cationization modes of GGG, involving various combinations of the carbonyl oxygens and the terminal amine nitrogen. The results are shown in Fig. 3. Conformers **1–3** maximize the peptide-cation electrostatic interactions with all three carbonyls coordinated to sodium. In addition, the terminal amine is bound to Na^+ in **1**. The difference between **2** and **3** lies in the orientation of the central C=O bond interacting with the cation, relative to the other two. In both cases the carbonyls are oriented towards Na^+, but the difference in conformation leads to a more compact structure for **2**. The distance between the oxygen of the carbonyls of first and last glycine residue is 3.53 Å while it is 4.05 Å in **3**. In agreement with previous work [54], structures **1–3** are the lowest in energy, as confirmed here at the B3LYP/6-311+G(2d,2p)//B3LYP/6-31G* level (see Fig. 3). Among the three, **1** is the least stable.

Conformer **4** also bears three carbonyl-sodium interactions, yet it has a more compact structure since the terminal acid is a hydrogen bond donor towards the terminal amine. The three

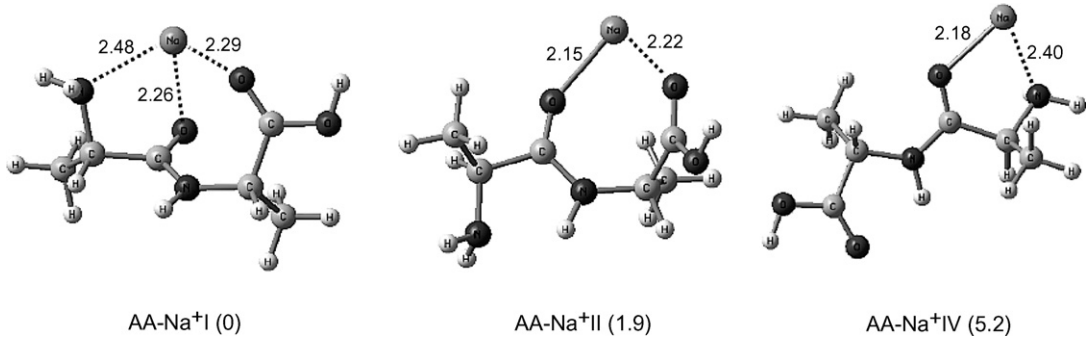

Fig. 2. Computed structures for the most stable diastereoisomers of AA–Na^+ at the B3LYP/6-31G* level. The enthalpies (relative to that of structure **1**) are in kJ/mol, as calculated at the B3LYP/6-311+G(2d,2p)//B3LYP/6-31G* level. Bonds distances are given in Å.

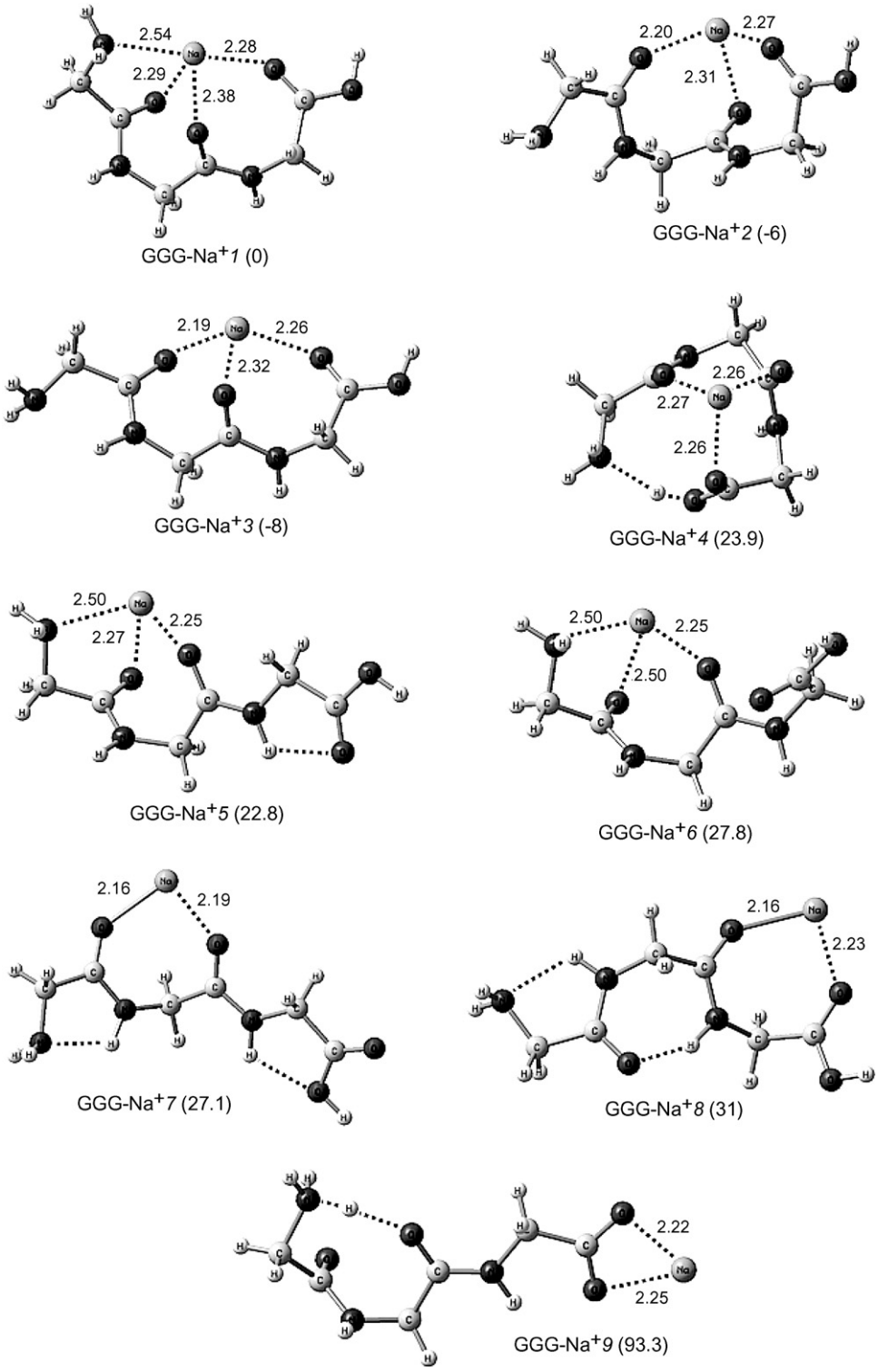

Fig. 3. Computed structures for GGG–Na^+ at B3LYP/6-31G* level. The enthalpies (relative to that of structure **1**) are in kJ/mol, as calculated at the B3LYP/6-311+G(2d,2p)//B3LYP/6-31G* level. Bonds distances are given in Å.

carbonyls are roughly parallel and oriented towards the metal. This structure is significantly higher in energy than **1**–**3**. Transfer of the acidic proton in **4** to the amine would lead to a zwitterion, which was identified at the HF/PB1 level, but could not be optimized with B3LYP/6-31G*, since it collapses towards **4**. Structures **5** and **6** are very similar, with two carbonyls and the terminal amide interacting with Na^+. The difference in energy is due to the stabilizing effect of the hydrogen bond between the C-terminus acid and the next peptidic N–H in **5**. All other conformers found are higher in energy, probably due to a lower

coordination number to the metal ion. For example, the structure of conformer **9** is a salt-bridge in which the sodium interacts only with the two oxygens of the carboxylate, and where a H-bond is formed between the ammonium and the oxygen of the central C=O bond. It is 93.3 kJ/mol higher in enthalpy than **1**. Other salt-bridge structures with a folded chain to allow a direct interaction of ammonium with one of the oxygen atoms of the carboxylate are even less stable.

In conclusion, conformers **1**–**3** are the most stable for GGG–Na^+ and in all three structures, Na^+ interacts with the three carbonyl oxygens. Changing the conformation at the N-terminus leads to small energy changes.

3.1.4. AAA–Na^+

The most stable structures of AAA–Na^+, including pairs of diastereoisomers, are shown in Fig. 4. As for GGG–Na^+, structures involving chelation of Na^+ to all three carbonyl oxygens are much more stable than all others, which are therefore not shown. There are slight differences in energy ordering between GGG–Na^+ and AAA–Na^+. This is due to the fact that when two consecutive carbonyls with parallel dipoles are coordinated to sodium the geometry is close to a γ-turn (C_7). There is an optimal equatorial position for the methyl group which minimizes the steric interactions. This is illustrated in Fig. 4 for conformer **2** and **2-diast** whose methyl groups are in equatorial and axial

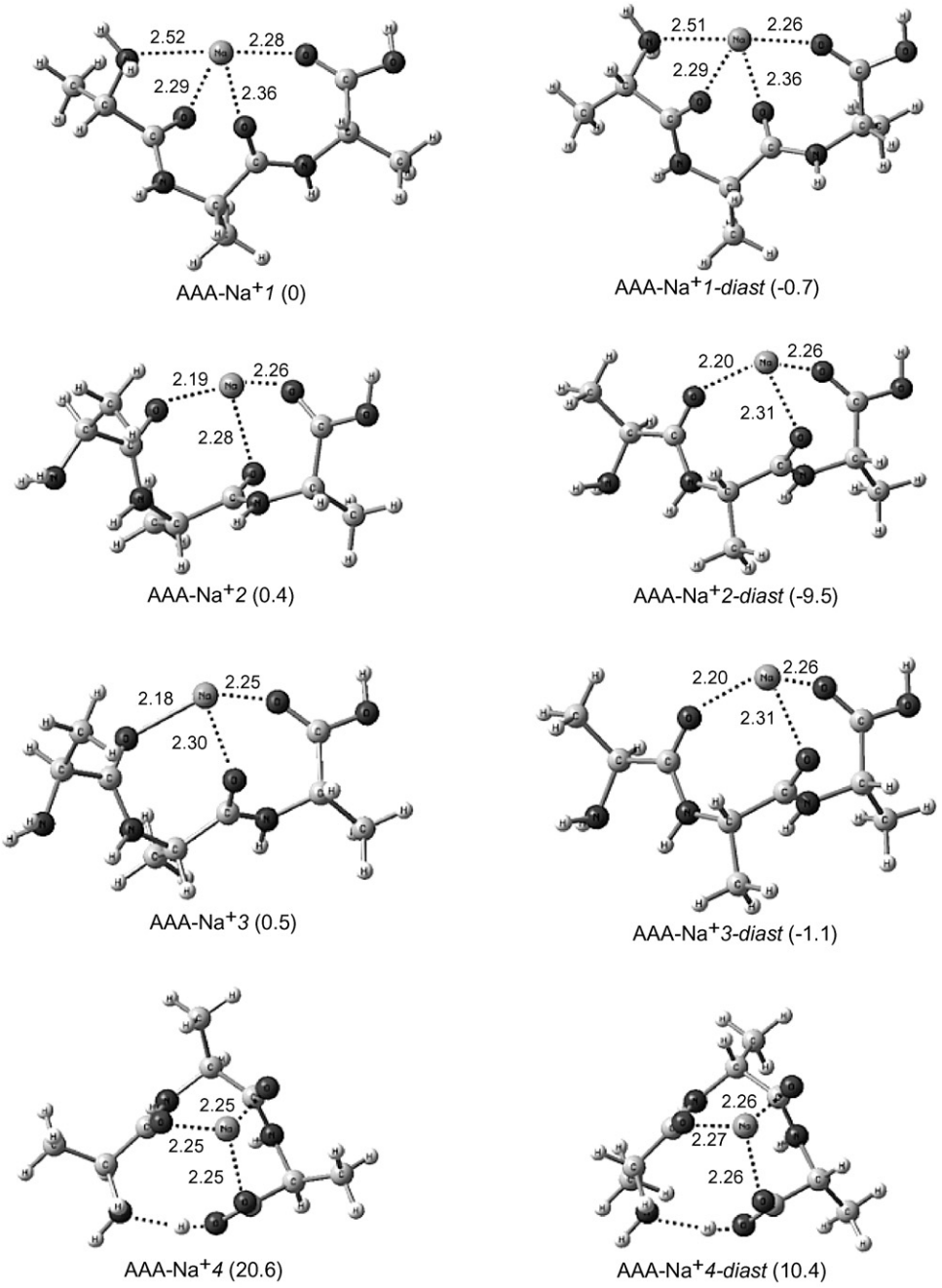

Fig. 4. Most stable structures of AAA–Na^+, including diastereoisomers. The enthalpies (relative to that of structure **1**) are in kJ/mol, as calculated at the B3LYP/6-311+G(2d,2p)//B3LYP/6-31G* level. Bonds distances are given in Å.

position, respectively. In the case of the two diastereoisomers of **1**, the carbonyls interacting with the cation have non-parallel dipole moments, the C_7 cycle is deformed and there is no clearly stabilizing or destabilizing position for the methyls (see Fig. 4). Conformer **4** is also shown. Its relative energy is very similar to its analogue for GGG–Na^+. However here again, the more favorable axial positions of the methyls make its diastereoisomer **4-diast** much more stable, although it is still 20 kJ/mol less stable than **2-diast**.

3.2. IRMPD spectra obtained in FT-ICR and RF trap experiments

Under irradiation with IR photons, elimination of Na^+ is a fragmentation that is common to all peptide–Na^+ ions. The appearance of bare Na^+ is clear in the spectra taken with MICRA, where it is the only fragmentation process of GG–Na^+ as shown in Fig. 5. Despite our best efforts, there is no Na^+ peak visible in the spectra recorded with the ion trap. However, under irradiation a clear decrease in the intensity of the parent ion occurs. Moreover there are no other significant peaks concomitant with the depletion of the parent signal. Although IRMPD is not plagued with the problems of classical CID experiments (mass cutoff at one third of the molecular ion mass [58–60]), the low mass of sodium ion, $m/z = 23$, places it near the lower detection limit of the machine, making it undetectable using our ion trap setup. As a consequence, the fragmentation ratio R cannot be calculated from the ion trap data for GG–Na^+ and AA–Na^+ thus parent depletion spectra are used.

For the larger GGG–Na^+ and AAA–Na^+, mass spectra show that although the loss of Na^+ is still the main fragmentation process, fragments corresponding to the loss of one H_2O molecule are present. Sequential loss of one and two amino acid molecules is also visible, leading to easily identifiable GG–Na^+ or AA–Na^+, and G–Na^+ or A–Na^+, respectively.

Despite the multiphotonic character and complexity of the IRMPD process, a satisfactory agreement with the computed linear absorption IR spectra has been observed for all four peptides presented here, as in most cases described previously in the literature. We have compared the parent depletion spectra of the four peptides with the computed IR absorption spectra of the lowest energy structures. The resolution of the IRMPD spectrum depends on the experimental conditions. A number of contributing causes, like the variation of the number of parent ions generated by the electrospray source and subsequently captured inside the ion trap, lowered the quality of the spectra. Therefore, only the most intense bands are taken into account. However one should note that the most valuable information is provided by the band positions rather than by their intensities. We used a rather high intensity of the IR laser, thus depleting more than 50% of the parent ions on the more intense bands, to ensure that depletion bands are visible, intense and could not be mistaken for a decrease in the intensity of the parent ions due to signal instability. This choice is likely to induce a broadening effect of the bands due to the high laser power and therefore to decrease the quality of the ion trap depletion spectra.

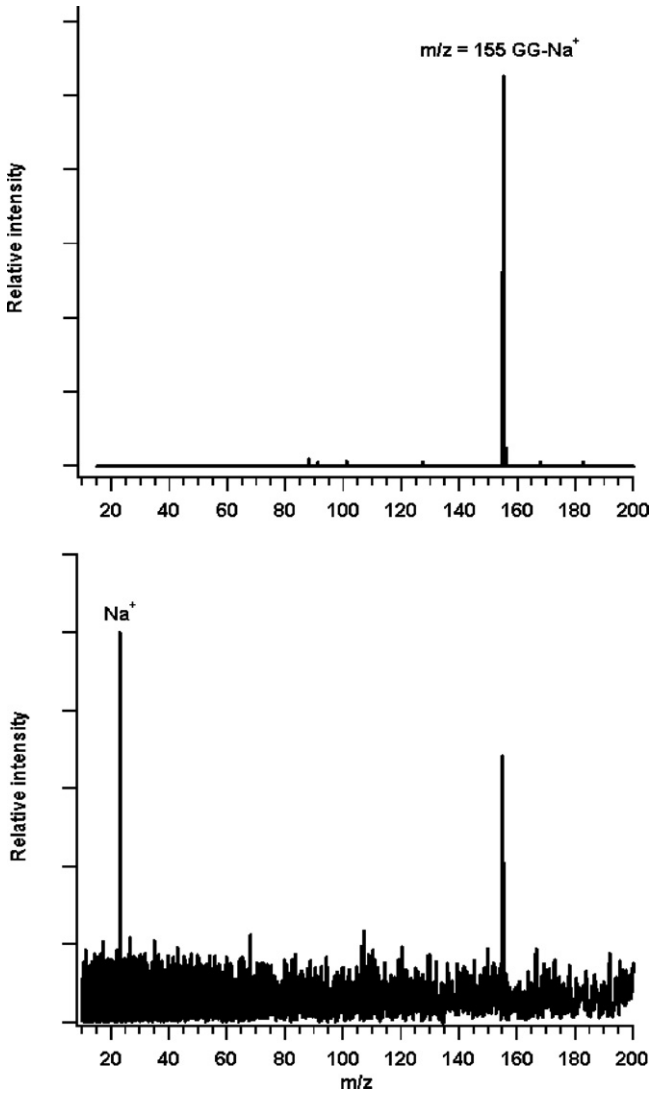

Fig. 5. Mass spectra of mass-selected GG–Na^+ under IR irradiation in both experimental setups. (Top) RF-trap Esquire, no Na^+ fragment detected. (Bottom) ICR trap MICRA, Na^+ is the only fragment ion detected.

In order to verify the reliability of parent depletion spectra obtained with the RF trap we have repeated the experiments using MICRA, which has the capability to detect low mass ions including Na^+, enabling the generation of parent fragmentation, rather than depletion spectra, which are usually less noisy. On the other hand, the ions were internally generated by MALDI, which requires constant vaporization of sample material and ion generation by the YAG laser, making it technically difficult to record a complete scan of the fingerprint region. In conclusion, we use the experimental fragmentation ratio spectra taken with MICRA to validate, confirm and detail the experimental parent depletion spectra obtained with the ESQUIRE ion trap.

3.2.1. GG–Na^+

The comparison of the depletion spectrum of GG–Na^+ recorded in the ion trap with the IR absorption spectra computed for the lowest energy structures is done in Fig. 6. The IRMPD spectrum is well consistent with the calculated IR spectra of

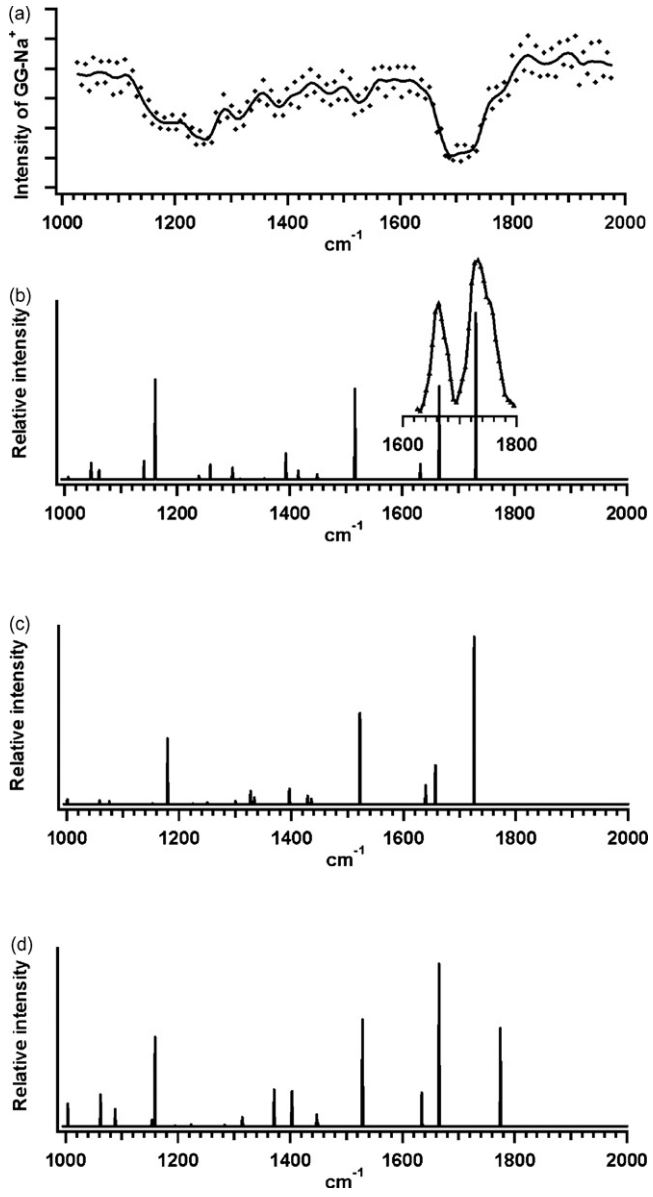

Fig. 6. (a) Depletion spectrum of GG–Na^+ in the ion trap, as processed using a binomial smooth. (b)–(d) Computed absorption spectra for structures **I**, **II**, and **IV**, respectively, at the B3LYP/6-31G* level using a scaling factor of 0.96. The MICRA-IRMPD (ICR trap) fragmentation spectrum in the 1600–1800 cm^{-1} range is shown as an insert in (b).

the lowest energy structures **I** and **II** (see Fig. 6 and Table 1, in which the full MICRA fragmentation spectrum is described). Although the resolution of the parent depletion spectrum is not excellent (around 60 cm^{-1}), its major characteristics are easily identifiable: an intense and large band at 1120–1280 cm^{-1} which appears to correspond to unresolved intense bands at 1180 and 1260 cm^{-1}, and a second intense band at 1640–1780 cm^{-1} which we also believe to be the convolution of two bands at 1660 and 1730 cm^{-1}. Probably due to the high laser power used, the clearly separated bands (as seen in the MICRA spectrum) have suffered a broadening effect and overlapped, the result being the large band seen in Fig. 6(a). The 1300–1600 cm^{-1} region is relatively noisy. It is not obvious that there are any real bands in this range although it is tempting to associate the "feature" at 1510–1550 cm^{-1} with the intense lines computed at 1516, 1523 and 1529 cm^{-1} for **I**, **II** and **IV**, respectively. Thus none of the bands in the 1000–1600 cm^{-1} range can be structurally diagnostic. The only clear difference among the most intense lines in (b)–(d) lies in their position and intensity in the 1600–1800 cm^{-1} region. These bands can be assigned to the C=O stretch, encompassing the amide I band typical of peptides, and the analogous mode of the C-terminal acid. The amide I band is computed at 1656 for **II** and 1666 for **I** and **IV**, respectively. In all three structures, the amide C=O interacts with Na^+ in fairly similar ways, leading here again to similar intensities. However the acidic C=O is bound to Na^+ in **I** and **II** but not in **IV**, leading to a blue-shift of ca. 50 cm^{-1} in the latter case (1775 cm^{-1} vs. 1731 cm^{-1} and 1726 cm^{-1} for **I** and **II**, respectively). The IRMPD spectrum obtained with MICRA has better resolution in this area and allows us to conclude that structure **IV** is not present, since there is no experimental peak visible around the theoretically intense 1775 cm^{-1}, as can be seen in Fig. 6. Any peak in that region would be easily seen in the fragmentation spectrum as it would lead to a greater separation between the two intense bands. The C=O stretching frequency difference induced by coordination to sodium thus provides an easy tool to distinguish between structures that have either one or both carbonyls bound to the ion.

On the other hand there is no possibility to clearly distinguish between conformers **I** and **II** on the basis of their IRMPD spectra. One could argue that only conformer **I** is present since the relative intensities of the theoretical peaks at 1665 and 1730 cm^{-1} fit rather well with those of experimental IRMPD peaks at 1663 and 1732 cm^{-1}. However there is precedent [5,6] showing that IRMPD intensities cannot be directly compared to computed absorption intensities, especially for nearby peaks.

3.2.2. AA–Na^+

AA–Na^+ was analyzed exclusively by IRMPD in MICRA. The resulting spectrum, rather similar to that of GG–Na^+ discussed above, is presented in Fig. 7 and described in Table 1. It displays four intense bands. The first large and intense band at 1100–1200 with the maximum intensity at 1161 cm^{-1} may be associated with the C–O–H bend mode for all conformers. However in the case of structure **IV**, another band of high intensity exists at 1113 cm^{-1}, which together with the band at 1164 cm^{-1} yields a double profile characteristic for **IV**. It is identified as one collective intense $\omega\,NH_2 + \upsilon\,C{-}N + \tau\,NH$ mode (other combinations of these local modes are much less intense). Similar collective modes were also present for structure **IV** of GG–Na^+ but less intense (75 km/mol vs. 136 km/mol). The absence of this band from the experimental spectrum argues against a significant population of **IV**, thus indicating a predominant presence of **I** and **II**. The bands at 1511 and 1660 cm^{-1} correspond to amides II and I modes, respectively. The theoretical bands of the three conformers are close enough in value that these bands do not allow us to differentiate between the structures. However, as discussed above for GG–Na^+, the acidic C=O stretch band at 1730 cm^{-1} is compatible with the bands of **I** and **II** at 1721 and 1726 cm^{-1} but not with the one of **IV** at 1765 cm^{-1}. In conclu-

Table 1
Experimental and computed vibrational band intensities for GG–Na^+ and AA–Na^+

GG-Na^+						AA-Na^+				
Frequency (cm^{-1})		Computed intensity (Km/mol)			Mode	Computed intensity (Km/mol)			Frequency (cm^{-1})	
Exp band	Calc	I	II	IV		I	II	IV	Calc	Exp band
	1003			53	ω NH_2 + ν C-N + τ NH …	52			1022	
	1046	37						32	1074	
	1063			75		58			1110	
	1088			40				136	1113	
	1140	41					38		1123	
	1159			212	ν C-O-H + δ C-O-H	222			1163	**1100-1200 (1161)**
	1161	223						134	1164	
1120-1280 (1180, 1260)	1180		203				206		1174	
	1259	32			ω NH + ω CHR + δ R + δ COH + …	58			1221	
	1328		40			47			1312	
	1372			87			44		1336	
1380-1400 (1390)	1393	57						102	1347	
	1397		48					31	1395	
	1404			83			49		1396	
					2 δ CH_3			41	1461	
	1516	201			ω NH + ω CHR + δ R + δ COH + …	196			1516	**1485-1530 (1511)**
1510-1550 (1530)	1523		282					262	1524	
	1529			253			299		1525	
	1633	34			δ NH_2	40			1625	
	1634			80				86	1628	
	1640		58				57		1634	
	1656		120		ν C=O		103		1650	**1640-1670 (1660)**
1640-1680 (1663)	1666			385				317	1654	
1640-1780 (1700)	1666	208				163			1661	
	1726		519		ν C=O (acid)	372			1721	**1710-1760 (1730)**
1710-1770 (1732)	1731	371					460		1726	
	1775			232				229	1765	

The wavenumbers in parentheses correspond to the maximum(a) of the experimental bands. In bold, the bands of the spectrum obtained with the ICR trap (MICRA) and in italics the bands of spectrum obtained with the ion trap (Bruker Esquire).

sion, the IRMPD spectrum allows excluding the formation of conformer **IV**, but cannot differentiate between the lowest two conformers.

3.2.3. GGG–Na^+

There is a strong resemblance between the theoretical IR spectra of conformers **1**–**3** in the case of GGG–Na^+. They are characterized by four intense absorption bands: the C–O–H bend from 1158 to 1163 cm^{-1}, the amide II band from 1499–1532 cm^{-1}, the amide I band between 1652 and 1687 cm^{-1}, and the carboxylic acid C=O stretch in the 1740–1776 cm^{-1} range. The main structural difference between the three conformers is the position of the terminal NH_2–CH_2 whose associated vibrations are weak. This results in very similar theoretical IR spectra. Due to the limited resolution of IRMPD at room temperature it would be difficult to make a difference between these three conformers. Thus, out of three, only the spectrum computed for conformer **2** is shown in Fig. 8. The spectrum computed for conformer **4** was added, as a representative of a higher energy structure, which also has all three carbonyl oxygens bound to sodium.

The experimental depletion and fragmentation IRMPD spectra and the calculated IR spectra for two of the GGG–Na^+ conformers are shown in Fig. 8. The signal to noise ratio of the fragmentation spectrum is worse than that of the parent depletion spectrum however this may be due to the congestion of the absorption bands. In the region between 800 and 2000 cm^{-1} about 30 theoretical absorption bands for each conformer can be counted. Those having intensities larger than 30 km/mol and their assignment are detailed in Table 2. The experimental IRMPD and ion depletion spectra are very similar and display four intense absorption bands having their maxima around 1160, 1520, 1690 and 1760 cm^{-1}.

The band at 1160 cm^{-1} is assigned to the C–O–H bend for conformers **1**–**3** and **5** giving an excellent concordance between the theoretical and experimental frequencies. Conformer **4** does not have any calculated band in this region.

Just next to it, a band of lower intensity at 1210–1290 cm^{-1} is assigned to the bending vibration of the neighbouring peptide NH and CH_2 (see Table 2). Unfortunately all the conformers have theoretical bands in this region and the width of the band may suggest the presence of more than one con-

Table 2
Experimental and computed vibrational band intensities for GGG–Na^+

GGG-Na^+							
Frequency (cm^{-1})		**Computed intensity (Km/mol)**					**Mode**
Exp.	**Calc.**	**1**	**2**	**3**	**4**	**5**	
	1037				51		delocalized
	1041					31	ω NH_2 + ν C-N + …
	1046	30					
	1049				48		delocalized
	1083				239		
	1088					35	ω NH_2 + ν C-N + …
	1158					233	
1130-1200	1160		268				ν C-OH + δ C-O-H
(1160)	1162	292					
	1163			295			
	1207				49		delocalized
	1212			57			
	1213	43					
1210-1290	1238				42		ω NH + ω CH_2 + δ C-O-H + …
(1230)	1257	33					
	1259			44			
	1263				71		delocalized
	1265					43	ω NH + ω CH_2 + δ C-O-H + …
	1280		46				
	1296				107		delocalized
	1319				61		ω NH + ω CH_2 + δ C-O-H + ν C-N …
	1321		41				
	1345					63	
	1350			48			
	1396	40					
	1397		44				
	1398					139	
				45			
	1499				149		
	1505	178					
	1507				179		
	1512		265				
1470-1570				249			
(1520)	1515		200				
	1517					154	
		222					
	1520					314	
	1532			262			
	1602				111		
	1631	42					δ NH_2
	1633					33	
	1638			68			
	1640		51				
	1652					298	
	1655			249			
	1661		71				2 ν^{as} C=O
1630-1714	1664	288					
(1690)	1665				31		
	1681	85					
	1682		358				2 ν^{s} C=O
	1685					407	
	1687			176			
	1718				656		3 ν^{s} C=O
	1740			400			
1714-1790	1744		406				ν C=O (acid)
(1760)	1746	397					
	1776					230	

The wavenumbers in parentheses correspond to the maximum(a) of the experimental bands. The same positions were observed with the ICR trap (MICRA) and with the RF trap (Bruker Esquire). The latter are given in italics.

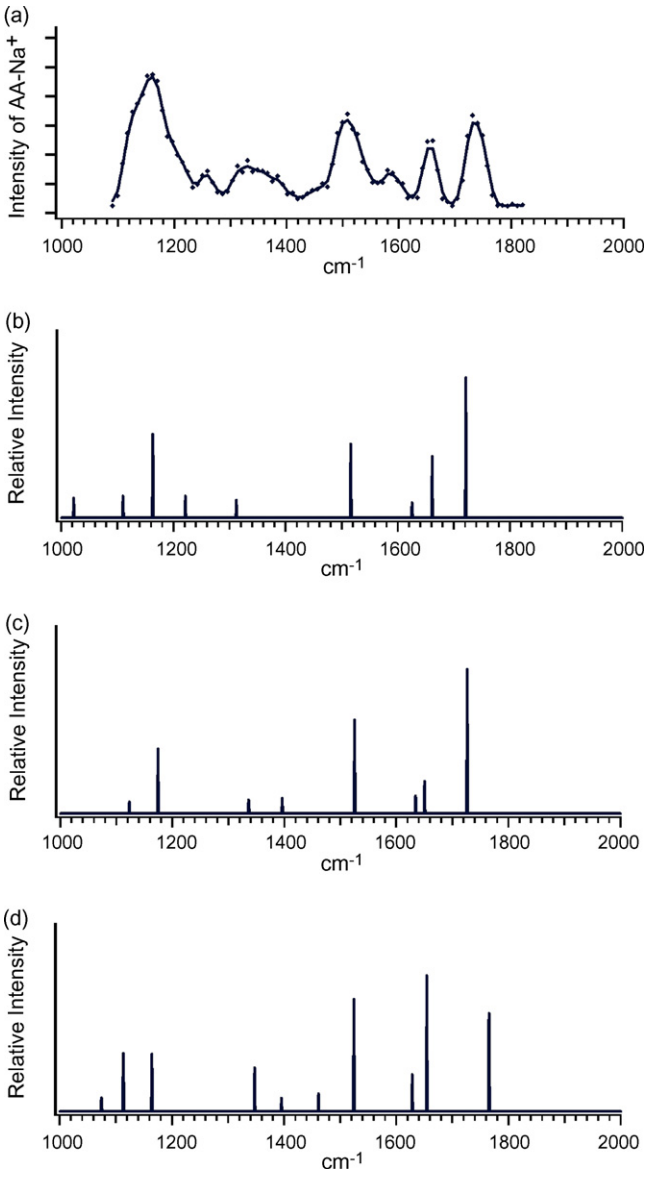

Fig. 7. (a) IRMPD fragmentation spectrum of AA–Na^+ recorded in the ICR trap (b)–(d) Computed IR absorption spectra for structures **I, II** and **IV** of AA–Na^+ at the B3LYP/6-31G* level using a scaling factor of 0.96. The fragmentation spectrum was processed using a binomial smooth.

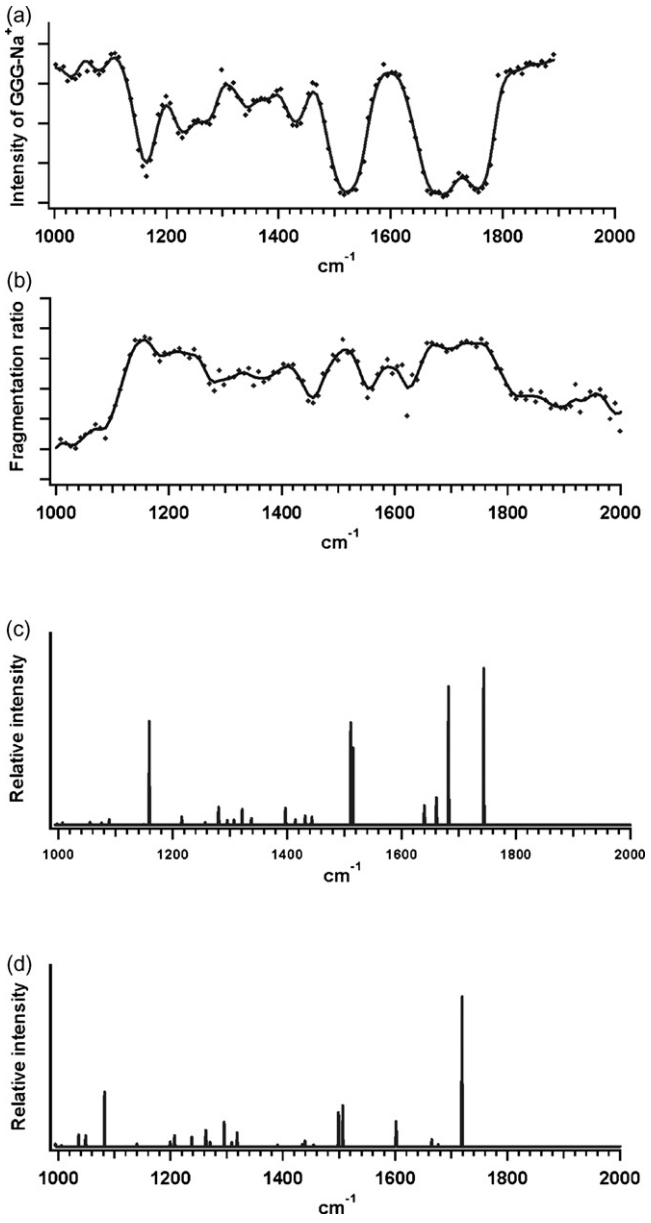

Fig. 8. (a) IRMPD depletion spectrum of GGG–Na^+ recorded in the ion trap. (b) IRMPD fragmentation spectrum of GGG–Na^+ recorded in the ICR trap. (c) and (d) Computed IR absorption spectra for structures **2** and **4** of GGG–Na^+ at the B3LYP/6-31G* level using a scaling factor of 0.96. The depletion and fragmentation spectra were processed using a binomial smooth.

former. The band with the maximum at 1510 cm^{-1} in the fragmentation spectrum and 1520 cm^{-1} for the parent depletion spectrum, corresponding to a coupling of the angular deformation between the peptide NH, the neighbouring CH_2 and of C–OH, is common to all conformers and therefore is not specific.

As for the dipeptides, the amide and acid C=O stretching frequencies are in the 1600–1800 cm^{-1} region. The experimental double band profile is characteristic for conformers **1**–**3** and **5**. However in the case of **5** the terminal acid is not interacting with the cation. Thus its stretching is shifted towards higher frequencies leading to a bigger band separation than for the other three conformers. Thus if formed, it would lead to an experimental band that would be either much larger than it is, or separated into two bands. Since there is no absorption at 1776 cm^{-1} in either experimental spectra, formation of **5** can be excluded. In this wavelength range, the experimental results cannot exclude the presence of conformer **4**. The latter has all three C=O bonds nearly parallel, therefore their stretches are strongly coupled, contrary to the other conformers in which the acid carbonyl stretch remains uncoupled with those of the amides. In this parallel arrangement, there is only one amide I mode of large intensity, that in which the three C=O stretches are coupled in phase. Any out of phase component corresponds to a much reduced dipole moment variation and therefore a small IR intensity. The presence of conformer **4** to a significant extent can be ruled out because the experimental spectrum shows no feature at 1083 cm^{-1} (amine umbrella motion coupled to a COOH tor-

Table 3
Experimental and computed vibrational band intensities for AAA–Na^+

AAA-Na^+							
Frequency (cm^{-1})		Computed intensity (Km/mol)					Mode
Exp.	Calc.	1	2	3	4	5	
	1037	34					ω NH_2 + ν C-N + ω CH_3 …
	1050				160		
	1061				114		
	1084				43		
	1100					48	
	1126					92	
			102				
	1131				85		delocalized
	1135	107					ω NH_2 + ν C-N + ω CH_3 …
	1145			160			
1120-1200 (1180)	1162					131	ν C-OH + δ C-O-H
			205				
	1174			110			
	1176	139					
	1179				36		delocalized
	1212				83		
	1216	102					ω NH + ω CH_2 + δ C-O-H + ν C-N + ω CH_3 + …
	1222			33			
	1223					82	
	1227		65				
	1232				237		
	1301			51			
	1314		62				
	1324				64		
	1332				63		
	1346					54	
	1352	44					
	1354					85	
	1359			35			
	1384					45	
	1393					32	
	1462					55	
	1464	36					
	1467			36			
	1498				138		
	1505			298			
1460-1570 (1510)	1506	217					
	1507				161		
	1510	196					
	1512		248				
			222				
	1517					72	
	1519					391	
	1529			265			
	1597				105		δ NH_2
	1623	69					
	1626					42	
	1634		53				
	1635			77			
	1643			202			2 ν^{as} C=O
						226	
	1650	231					
1640-1720 (1680)	1652		73				
	1667	109					
	1668			198			2 ν^{s} C=O
	1678		286				
	1680					303	
	1716				551		3 ν^{s} C=O
	1727			395			ν C=O (acid)
1720-1790 (1755)	1732	394					
	1742		400				
	1767					223	

The wavenumbers in parentheses correspond to the maxima of the experimental bands obtained with the ion trap (Bruker Esquire).

sion), where it is predicted to have significant absorption, while **1**–**3** do not.

As a result, although we can eliminate conformers **4** and possibly **5**, we cannot differentiate between conformers **1**–**3**. The high energy of **5** makes its presence rather unlikely, however.

3.2.4. AAA–Na^+

As for GGG–Na^+, the IR theoretical spectra of **1**–**3** conformers are remarkably similar as can be seen in Table 3. There are four most intense absorption bands common to all three conformers: the C–O–H bend in the 1162–1176 cm^{-1} region, the amide II mode from 1498 to 1529 cm^{-1}, the amide I mode between 1643 and 1680 cm^{-1} and the acidic C=O stretch from 1727 to 1742 cm^{-1} (see Table 3). There are small differences in the frequencies and intensities of the theoretical bands in the 1000–1300 cm^{-1} region, which correspond to delocalized modes with significant components of the angular deformations of the methyl groups. Due to the very small difference between the three conformers and the accessible resolution in the IRMPD spectra, it is impossible to identify any diagnostic difference between the three structures. Therefore, as for GGG–Na^+, we chose to show only the computed spectrum of conformer **2** as representative for all three (see Fig. 9). The experimental parent depletion spectrum consists of four bands, at 1120–1200 cm^{-1} with a maximum at 1180, 1460–1570 cm^{-1} with a maximum at 1510 cm^{-1} and a feature in the 1640–1790 cm^{-1} region with two components of equal intensity having their maxima at 1680 and 1755 cm^{-1}, respectively. The double band is a major feature of the spectrum and by itself allows to rule out the formation of conformers **4** and **5**. Both of them have only one band in that region, at 1716 cm^{-1} for **4** and 1767 cm^{-1} for **5**. The result is that the profile of this band and the frequency difference in the C=O stretch region is compatible with conformers **1**–**3** only. Moreover, the absence of parent depletion around 1050–1060 cm^{-1} shows that conformer **4** is absent. Again, due to the strong resemblance between the computed vibrational features of conformers **1**–**3**, the present IRMPD results do not allow for single conformer identification.

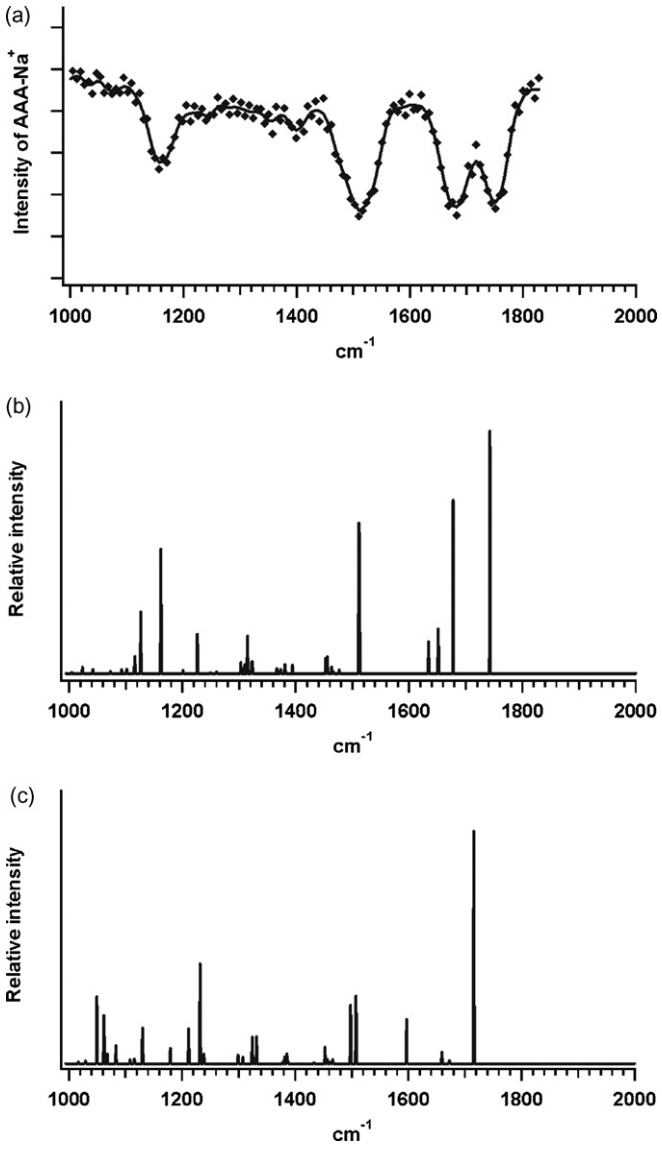

Fig. 9. (a) IRMPD depletion spectrum of AAA–Na^+. (b) and (c) Computed IR absorption spectra computed for structures **2** and **4** of AAA–Na^+ at the B3LYP/6-31G* level using a scaling factor of 0.96. The depletion spectrum was processed using a binomial smooth.

4. Conclusion

We have recorded depletion and fragmentation IRMPD spectra for sodiated di- and tripeptides of glycine and alanine in the fingerprint region. Based on computed IR absorption spectra band assignment was straightforward in most cases.

The present work shows that IRMPD spectroscopy is an efficient method to distinguish between conformers which differ by their numbers of carbonyls interacting with the cation. It is also easy to distinguish structures in which the C-terminus is H-bonded to the N-terminus. However the present method cannot distinguish between the conformers of the same class, such as **I** and **II** for AA–Na^+ or GG–Na^+ or **1**–**3** for AAA–Na^+ and GGG–Na^+.

Identification of each single conformer may be possible with higher resolution spectra, which could be achieved by cooling ions in the trap. This experimental extension is currently underway. Another possibility may be to probe ion absorptions in the 3000–4000 cm^{-1} region, using an OPO laser rather than a FEL. Such a device is now in operation at CLIO.

Acknowledgements

We thank Dr. Jean Michel Ortega and the CLIO team for technical assistance. O.-P. Balaj was supported by a postdoctoral fellowship from Ecole Polytechnique and from the STREP EPITOPES funded by the 6th European Program of Research and Development. We are grateful to the Institut de Développement et de Ressources en Informatique Scientifique (IDRIS) for generous allocation of computer resources (Grant no. 0543).

References

[1] R.L. Woodin, D.S. Bomse, J.L. Beauchamp, J. Am. Chem. Soc. 100 (1978) 3248.
[2] R. Prazeres, F. Glotin, C. Insa, D. Jaroszynski, J.M. Ortega, Eur. Phys. J. D 3 (1998) 87.
[3] D. Oepts, A.F.G. van der Meer, P.W. van Amersfoort, Infrared Phys. Technol. 36 (1995) 297.
[4] J. Oomens, A.J.A. van Roij, G. Meijer, G. von Helden, Astrophys. J. 542 (2000) 404.
[5] J. Oomens, B.G. Sartakov, G. Meijer, G. von Helden, Int. J. Mass Spectrom. 254 (2006) 1.
[6] C. Kapota, J. Lemaire, P. Maître, G. Ohanessian, J. Am. Chem. Soc. 126 (2004) 1836.
[7] N.C. Polfer, J. Oomens, R.C. Dunbar, Phys. Chem. Chem. Phys. 8 (2006) 2744.
[8] N.C. Polfer, R.C. Dunbar, J. Oomens, J. Am. Soc. Mass Spectrom. 18 (2007) 512.
[9] N.C. Polfer, B. Paizs, L.C. Snoek, I. Compagnon, S. Suhai, G. Meijer, G. von Helden, J. Oomens, J. Am. Chem. Soc. 127 (2005) 8571.
[10] N.C. Polfer, J. Oomens, D.T. Moore, G. von Helden, G. Meijer, R.C. Dunbar, J. Am. Chem. Soc. 128 (2006) 517.
[11] J. Oomens, N.C. Polfer, D.T. Moore, L. van der Meer, A.G. Marshall, J.R. Eyler, G. Meijer, G. von Helden, Phys. Chem. Chem. Phys. 7 (2005) 1345.
[12] J. Oomens, D.T. Moore, G. von Helden, G. Meijer, R.C. Dunbar, J. Am. Chem. Soc. 3 (2004) 724.
[13] J. Oomens, G. von Helden, G. Meijer, J. Phys. Chem. A 108 (2004) 8273.
[14] D.T. Moore, J. Oomens, J.R. Eyler, G. von Helden, G. Meijer, R.C. Dunbar, J. Am. Chem. Soc. 127 (2005) 7243.
[15] D.T. Moore, J. Oomens, J.R. Eyler, G. von Helden, G. Meijer, D.P. Ridge, J. Am. Chem. Soc. 126 (2004) 14726.
[16] G.S. Groenewold, A.K. Gianotto, K.C. Cossel, M.J. Van Stipdonk, D.T. Moore, N.C. Polfer, J. Oomens, W.A. de Jong, L. Visscher, J. Am. Chem. Soc. 128 (2006) 4802.
[17] R.C. Dunbar, D.T. Moore, J. Oomens, J. Phys. Chem. A 110 (2006) 8316.
[18] T.D. Fridgen, T.B. McMahon, L. MacAleese, J. Lemaire, P. Maitre, J. Phys. Chem. A 108 (2004) 9008.
[19] B. Chiavarino, M.E. Crestoni, S. Fornarini, J. Lemaire, L. MacAleese, P. Maitre, Chem. Phys. Chem. 5 (2004) 1679.
[20] A. Simon, W. Jones, J.M. Ortega, P. Boissel, J. Lemaire, P. Maitre, J. Am. Chem. Soc. 126 (2004) 11666.
[21] O. Dopfer, N. Solca, J. Lemaire, P. Maitre, M.E. Crestoni, S. Fornarini, J. Phys. Chem. A 109 (2005) 7881.
[22] T.D. Fridgen, T.B. McMahon, P. Maitre, J. Lemaire, J. Phys. Chem. Chem. Phys. 8 (2006) 2483.
[23] B. Chiavarino, M.E. Crestoni, S. Fornarini, J. Lemaire, P. Maitre, L. MacAleese, J. Am. Chem. Soc. 128 (2006) 12553.
[24] B. Chiavarino, M.E. Crestoni, S. Fornarini, F. Lanucara, J. Lemaire, P. Maitre, Angew. Chem. Int. Ed. 46 (2007) 1995.
[25] L. MacAleese, A. Simon, T.B. McMahon, J.M. Ortega, D. Scuderi, J. Lemaire, P. Maitre, Int. J. Mass Spectrom. 249 (2006) 14.
[26] B. Lucas, G. Gregoire, J. Lemaire, P. Maitre, J.M. Ortega, A. Rupenyan, B. Reimann, J.P. Schermann, C. Desfrancois, Phys. Chem. Chem. Phys. 6 (2004) 2659.
[27] B. Lucas, G. Gregoire, J. Lemaire, P. Maitre, F. Glotin, J.P. Schermann, C. Desfrancois, Int. J. Mass Spectrom. 243 (2005) 105.
[28] D.C. Marinica, G. Gregoire, C. Desfrancois, J.P. Schermann, D. Borgis, M.P. Gaigeot, J. Phys. Chem. A 110 (2006) 8802.
[29] R.P. Grese, R.L. Cerny, M.L. Gross, J. Am. Chem. Soc. 111 (1989) 2835.
[30] R.P. Grese, M.L. Gross, J. Am. Chem. Soc. 112 (1990) 5098.
[31] L.M. Teesch, J. Adams, J. Am. Chem. Soc. 112 (1990) 4110.
[32] L.M. Teesch, J. Adams, J. Am. Chem. Soc. 113 (1991) 812.
[33] L.M. Teesch, R.C. Orlando, J. Adams, J. Am. Chem. Soc. 113 (1991) 3668.
[34] H. Zhao, A. Reiter, L.M. Teesch, J. Adams, J. Am. Chem. Soc. 115 (1993) 2854.
[35] T. Lin, G.L. Glish, Anal. Chem. 70 (1998) 5162.
[36] T. Lin, A.H. Payne, G.L. Glish, J. Am. Soc. Mass Spectrom. 12 (2001) 497.
[37] T. Wyttenbach, J.E. Bushnell, M.T. Bowers, J. Am. Chem. Soc. 120 (1998) 5098.
[38] T. Shoeib, A.C. Hopkinson, K.W.M. Siu, J. Phys. Chem. B 105 (2001) 12399.
[39] W.Y. Feng, S. Gronert, K.A. Fletcher, A. Warres, C.B. Lebrilla, Int. J. Mass Spectrom. 222 (2003) 117.
[40] H.A. Cox, R.R. Julian, S.-W. Lee, J.L. Beauchamp, J. Am. Chem. Soc. 126 (2004) 6485.
[41] V. Anbalagan, B.A. Perera, A.T.M. Silva, A.L. Gallardo, M. Barber, J.M. Barr, S.M. Terkarli, E.R. Talaty, M.J. Van Stipdonk, J. Mass Spectrom. 37 (2002) 910.
[42] V. Anbalagan, A.T.M. Silva, S. Rajagopalachary, K. Bulleigh, E.R. Talaty, M.J. Van Stipdonk, J. Mass Spectrom. 39 (2004) 495.
[43] V. Anbalagan, J.N. Patel, G. Niyakorn, M.J. Van Stipdonk, Rapid Commun. Mass Spectrom. 17 (2003) 291.
[44] K. Bulleigh, A. Howard, T. Do, Q. Wu, V. Anbalagan, M.J. Van Stipdonk, Rapid Commun. Mass Spectrom. 20 (2006) 227.
[45] A. Kamariotis, O.V. Boyarkin, S.R. Mercier, R.D. Beck, M.F. Bush, E.R. Williams, T.R. Rizzo, J. Am. Chem. Soc. 128 (2006) 905.
[46] M.F. Bush, J.T. O'Brien, J.S. Prell, R.J. Saykally, E.R. Williams, J. Am. Chem. Soc. 129 (2007) 1612.
[47] M. Kussmann, E. Nordhoff, H. Rahbek-Nielsen, S. Haebel, M. Rossel-Larsen, L. Jakobsen, J. Gobom, E. Mirgorodskaya, A. Kroll-Kristensen, L. Palm, P. Roepstorff, J. Mass Spectrom. 32 (1997) 593.
[48] J. Lemaire, P. Boissel, M. Heninger, G. Mauclaire, G. Bellec, H. Mestdagh, A. Simon, S.L. Caer, J.M. Ortega, F. Glotin, P. Maitre, Phys. Rev. Lett. 89 (2002) 273002.
[49] P. Maitre, S. Le Caer, A. Simon, W.D. Jones, J. Lemaire, H. Mestdagh, M. Heninger, G. Mauclaire, P. Boissel, R. Prazeres, F. Glotin, J.M. Ortega, Nucl. Instrum. Methods Phys. Res. A 507 (2003) 541.
[50] C.H.S. Wong, N.L. Ma, C.W. Tsang, Chem. Eur. J. 8 (2002) 4909.
[51] M. Benzakour, M. Mcharfi, A. Cartier, A. Daoudi, J. Mol. Struct.: Theochem 710 (2004) 169.
[52] B.A. Cerda, S. Hoyau, G. Ohanessian, C. Wesdemiotis, J. Am. Chem. Soc. 120 (1998) 2437.
[53] M.M. Kish, C. Wesdemiotis, G. Ohanessian, J. Phys. Chem. B 108 (2004) 3086.
[54] P. Wang, C. Wesdemiotis, C. Kapota, G. Ohanessian, J. Am. Soc. Mass Spectrom. 18 (2007) 541.
[55] C. Kapota, G. Ohanessian, Phys. Chem. Chem. Phys. 7 (2005) 3744.
[56] M.D. Halls, H.B. Schlegel, J. Chem. Phys. 109 (1998) 10587.
[57] M.J. Frisch, G.W. Trucks, H.B. Schlegel, G.E. Scuseria, M.A. Robb, J.R. Cheeseman, J.A. Montgomery Jr., T. Vreven, K.N. Kudin, J.C. Burant, J.M. Millam, S.S. Iyengar, J. Tomasi, V. Barone, B. Mennucci, M. Cossi, G. Scalmani, N. Rega, G.A. Petersson, H. Nakatsuji, M. Hada, M. Ehara, K. Toyota, R. Fukuda, J. Hasegawa, M. Ishida, T. Nakajima, Y. Honda, O. Kitao, H. Nakai, M. Klene, X. Li, J.E. Knox, H.P. Hratchian, J.B. Cross, V. Bakken, C. Adamo, J. Jaramillo, R. Gomperts, R.E. Stratmann, O. Yazyev, A.J. Austin, R. Cammi, C. Pomelli, J.W. Ochterski, P.Y. Ayala, K. Morokuma, G.A. Voth, P. Salvador, J.J. Dannenberg, V.G. Zakrzewski, S. Dapprich, A.D. Daniels, M.C. Strain, O. Farkas, D.K. Malick, A.D. Rabuck, K. Raghavachari, J.B. Foresman, J.V. Ortiz, Q. Cui, A.G. Baboul, S. Clifford, J. Cioslowski, B.B. Stefanov, G. Liu, A. Liashenko, P. Piskorz, I. Komaromi, R.L. Martin, D.J. Fox, T. Keith, M.A. Al-Laham, C.Y. Peng, A. Nanayakkara, M. Challacombe, P.M.W. Gill, B. Johnson, W. Chen, M.W. Wong, C. Gonzalez, J.A. Pople, Gaussian 03, Revision C02, Gaussian, Inc., Wallingford, CT, 2004.
[58] K.R. Jonscher, J.R. Yates, Anal. Biochem. 244 (1997) 1.
[59] A. Colorado, J.X.X. Shen, V.H. Vartanian, J. Brodbelt, Anal. Chem. 68 (1996) 4033.
[60] M.C. Crowe, J.S. Brodbelt, Anal. Chem. 77 (2005) 5726.